International Journal of Applied Glass Science 3 [3] 189–204 (2012)
DOI:10.1111/j.2041-1294.2012.00093.x

INTERNATIONAL JOURNAL OF
Applied Glass
SCIENCE

Melt Homogenization and Self-Organization in Chalcogenides-Part I

Siddhesh Bhosle, Kapila Gunasekera,* and Punit Boolchand*†

School of Electronics and Computing Systems, College of Engineering and Applied Science, University of Cincinnati,Cincinnati, Ohio 45221-0030

Matthieu Micoulaut

Laboratoire de Physique Theorique de la Matiere Condensee, Universite Pierre et Marie Curie,Boite 121, 4 Place Jussieu, 75252, Paris Cedex 05, France

An FT-Raman profiling method is developed to monitor growth of structural homogeneity of binary Ge_xSe_{100-x} melts in real time (t_R) non-invasively as starting materials are reacted over days. Raman spectra of quenched melts were acquired along a one inch long column of a sample in a quartz tube. In the first step of reaction, $t_R < 2$ days, Ge-rich crystalline- and glassy-phases form and coexist with Se-rich glasses. In the second step, t_R extending up to 7 days, local structures characteristic of melts/glasses form, and steadily homogenize as Ge and Se atoms diffuse. The process terminates when all Raman lineshapes taken along the length of a sample coalesce into *unique* profile. Several factors contribute to the long reaction time t_R for melts to homogenize, including liquid density difference of Ge and Se, diffusion controlled nanoscale mixing of melts, batch dryness, batch sizes, and laser spot size. Physical properties of such *homogeneous* Ge_xSe_{100-x} glasses are found to be quite different from their *inhomogeneous* counterparts realized after the first step of reaction. Slow homogenization of chalcogenides melts may occur generally. Variations in physical properties of chalcogenide glasses possessing nominally the same composition may have their origin in structural heterogeneity and purity.

Introduction

In glass science, since its inception, melts have been reacted and equilibrated above the liquidus, typically for times ranging from a few hours to a several tens of hours.[1–10] To the best of our knowledge there has not been a diagnostic structural probe to non-invasively track evolution of *melt* homogeneity in real time. Unlike crystalline solids that form at a distinct stoichiometry by seed growth in a melt, glasses form over a wide range of stoichiometry. Thus, a glass composition obtained by melt quenching can only be homogeneous if melts are homogeneously alloyed. And although much is known on the thermodynamics of glass forming melts[11] much less is known on the kinetics of

†punit.boolchand@uc.edu
*Member, The American Ceramic Society

homogenization of such melts. In probing physical properties of glassy solids as a function of chemical composition, homogeneity is paramount. Although some physical properties, such as variation of glass transition temperature with composition, $T_g(x)$, may withstand some glass heterogeneity, many other properties such as the variations in enthalpy of relaxation at T_g, molar volumes, Raman mode frequency, and refractive index, each may be smeared due to glass structural heterogeneity. The power of Raman profiling as a diagnostic tool to characterize melt structural heterogeneity was recently introduced.[12,13] One found that 2-g sized melts of the well-studied[1,4,7,14–18] Ge_xSe_{100-x} binary took at least 168 h (7 days) to homogenize on a scale of 10 μm when reacted at 950°C. How does a melt homogenize? What factors control the process of melt homogenization in chalcogenides? We address some of these issues in the present work. We also find traces of water can promote melt homogenization but the resulting wet glasses possess physical properties that are intrinsically quite different from those of their dry counterparts. Differences in T_g, molar volumes, and enthalpy of relaxation of T_g between dry and wet chalcogenides glasses can be traced to some of bridging Se sites in the former replaced by dangling [OH] and [H] ends in the latter. These considerations apply to oxide glasses as well,[19,20] and is a point of ongoing discussions. To establish the intrinsic physical behavior of network glassy alloys as a function of composition, it is crucial to synthesize *dry and homogeneous* samples. Glass homogeneity is required not only to explore the *basic science* of the disordered state of matter[21–24] but also the ultimate performance of *glass products in industry*.[25]

The Ge_xSe_{100-x} binary is perhaps one of the most thoroughly investigated chalcogenide glass systems.[1–10,12,14–18,26] The diagnostic role of the nonreversing enthalpy at T_g as a probe of homogeneity and purity of batch compositions has come to the fore as we will illustrate herein. These findings permit identifying physical properties of glasses that are *intrinsic* to these materials, to be distinguished from those that are *extrinsic* caused either by incomplete homogenization of a batch composition, or presence of water traces, or other network additives. Variation in the glass transition temperature, $T_g(x)$, in dry and homogeneous Ge_xSe_{100-x} samples is now accurately described in terms of a polynomial that can be used to predict a glass composition x as we show in Part II. In homogeneous glasses, the jump in C_p near T_g from the glass to the liquid ($\Delta C_p(x) = C_p(\text{liquid}) - C_p(\text{glass})$), deduced from the reversing heat flow in modulated DSC experiments, is found to be *independent of x* over a wide range of compositions, $10\% < x < 33.33\%$. These $\Delta C_p(x)$ results do not reveal the suggested[27] correlation between melt fragilities $m(x)$ at $T > T_g$, with $\Delta C_p(x)$ of glasses at $T < T_g$. On the other hand, melt-fragilities correlate well with enthalpy of relaxation $\Delta H_{nr}(x)$ at T_g deduced from the non-reversing heat flow in mDSC experiments.[28] The correlation between $m(x)$ and $\Delta H_{nr}(x)$ appears to be a promising avenue to understanding the fundamental nature of the glass transition.[29,30] Other fundamental issues come to the fore in homogeneous glasses, such as elastic phase transitions and nanoscale chemical phase separation transition, each of which becomes rather abrupt with composition in the Ge_xSe_{100-x} binary as we show in Part II.

Equilibrium Phase Diagram of Ge-Se binary

The equilibrium phase diagram of the Ge_xSe_{100-x} binary[31] appears in Fig. 1. In the Se-rich domain, there is a eutectic near $x = 5.5(5)\%$ of Ge at a $T = 212$°C. At the eutectic temperature a liquid of $Ge_{5.5}Se_{94.5}$, c-Se and c-$GeSe_2$ coexist as suggested by the solidus (horizontal line) at 212°C. The phase diagram shows that the liquidus (T_l) steadily increases (broken line) from 212°C at $x = 5.5\%$ to 742°C at $x = 33.3\%$, and serves as a guide in synthesizing glasses as we discuss later. Congruently melting stoichiometric crystalline compounds exist at $x = 0$ (c-Se),[32] $x = 33.3\%$ (α-$GeSe_2$ and β-$GeSe_2$),[16] and $x = 50\%$ (c-GeSe).[33] In addition, there is a metastable crystalline composition c-Ge_4Se_9[34] formed at $x = 30.7\%$. The structure of this metastable crystalline phase has a close bearing to that of α-$GeSe_2$. The metastable form present in the phase diagram plays a role in aging of homogenized glasses at $x > 26\%$ at elevated temperatures as we comment in Part II.

The phase diagram shows that when a melt of $Ge_{15}Se_{85}$ composition is cooled past the liquidus to $T = 300$°C, it will decompose into a liquid of $Ge_{10}Se_{90}$ composition and c-$GeSe_2$. Cooling it further to the Eutectic temperature of 212°C, will result in segregation of the sample into two macroscopic phases, which can be described by the following stoichiometric relation,

$$Ge_{15}Se_{85} = \alpha(Se) + (100 - \alpha)Ge_{1/3}Se_{2/3} \quad (1)$$

with $\alpha = 55\%$. Thus, it is quite reasonable to expect Ge_xSe_{100-x} melts in the $0 < x < 33.33\%$ range when

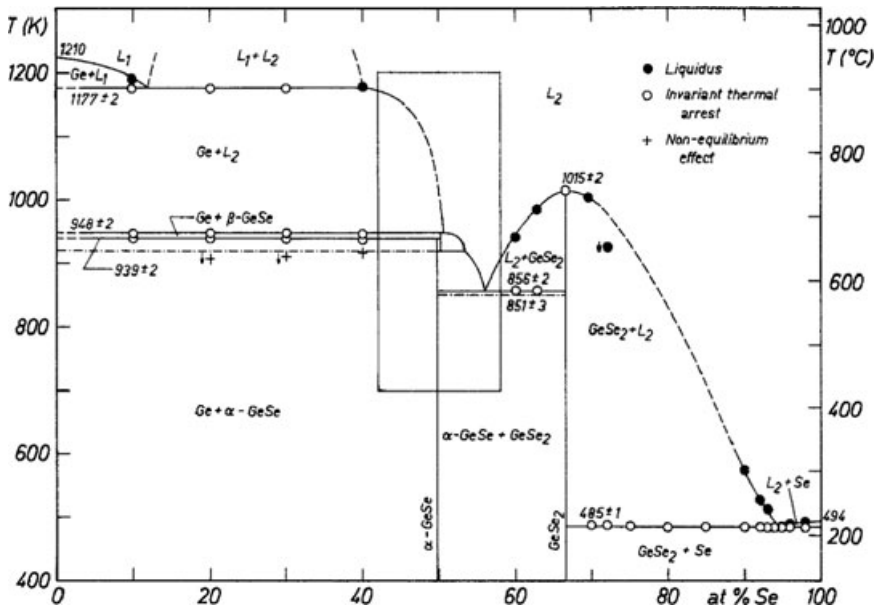

Fig. 1. Phase Diagram of the Ge_xSe_{100-x} binary taken from Isper et al.[31]

cooled across T_l to either (i) completely segregate to form c-Se and c-$GeSe_2$ upon slow cooling, or (ii) upon a fast quench to form a completely homogeneous glass of the melt stoichiometry and avoid decomposition. Alternatively, an intermediate circumstance can occur; the bulk glass formed may possess Se-rich and $GeSe_2$-rich regions that would result in microscopic heterogeneities (MH) determined by the considerations above (Fig. 1). In the next section we will describe synthesis of bulk glasses and show that, in general, at short reaction times (<6 h), melts are indeed, quite heterogeneous, and do indeed possess Se-rich and Ge-rich glassy regions, and even crystalline $GeSe_2$-rich regions. But as they are reacted for extended time, melts homogenize rather slowly if they are dry and quickly if they are wet, a process that we have monitored by Raman profiling the quenched melts.

Experimental Section

Synthesis of Ge_xSe_{100-x} Melts

Ge_xSe_{100-x} melts of 2 g in size were synthesized using 99.999% Ge and 99.999% Se pieces (3–4 mm diam) from Cerac Inc. The starting materials were mixed in the desired ratio by weight, sealed in evacuated (10^{-7} Torr) quartz tubing (5 mm ID) using a hydrogen/oxygen torch. The vacuum line consisted of a liquid nitrogen trapped high vacuum pumping system. Quartz tubes were washed with HF followed by de-ionized water and rapid drying. Prior to their use, tubes were dried in a vacuum oven at 90°C for 24 h. A total of 21 sample compositions spread in the $10\% < x < 33.33\%$ range of Ge were synthesized. The quartz ampoules were held vertically in a T-programmable box furnace for varying time periods, t_R, ranging from 6 h to 192 h at 950 °C largely to track and understand the evolving melt structure with position. In subsequent experiments melts were also physically rocked to promote mixing. It is useful to mention here that upon heating melts to 950°C, the liquid column was noted to reflux vigorously. Periodically *melts* were water quenched from 50°C above T_l (liquidus, Fig. 1) and examined in Raman profiling experiments (see below). Once homogenized, *as-quenched melts* in quartz tubes were taken to T_g +20°C in the box furnace, held there for 10 min, and then slow cooled to room temperature at 3°C/min to realize *homogeneous bulk glasses.*

Raman Profiling and Homogenization of Melts

All Raman profiling measurements on melts made use of a Thermo Nicolet NXR FT-Raman module

using 1064 nm radiation from an Nd-YAG laser with a laser spot size of 50 μm. The instrument has a motor stage that can be programmed to translate a sample by a pre-determined amount, and acquisition software to facilitate comparing spectra taken at different positions. Spectra were acquired at nine locations, spaced about 2.5 mm apart covering 25 mm length of the melt column. At each location, an acquisition took 7 min, and used 67 mW of laser power, with 200 scans yielding 2/cm resolution. A typical profiling scan, involving spectra acquired at the nine locations, took approximately an hour of accumulation time. Profiling experiments were performed at all the 21 compositions after reacting them for about 192 h, and in each case melts were found to be homogeneous on a scale of 10 μm (see below). At three compositions, x = 15%, 19%, and 33.3%, data were recorded as a function of t_R over 192 h to monitor growth of melt homogeneity. These results provide a unified view of melt homogenization.

The exciting radiation of 1.16 eV used in FT-Raman is near the middle of the optical gap[35] of Ge_xSe_{100-x} glasses, and is transparent to melts profiled in the experiments. However, because of the use of a notch filter to suppress the laser line, the low frequency (<100/cm) vibrational densities of states (VDOS) are inaccessible in FT-Raman experiments. The radiation excites electronic states deep in the gap,[36–38] which originate from "defects" in these glasses. For that reason, the full width at half maximum of the Corner-Sharing (CS) $GeSe_4$ vibrational mode near 200/cm in the spectra of homogenized melts/glasses are found to be substantially broadened (17–30% across the range of compositions from 10% < x < 33.33%) compared to the ones in dispersive Raman ones using 647 nm excitation from a Kr-ion laser. The mode broadening leads to a general smearing of the elastic phase transitions.[39,40] Thus, while the Thermo Nicolet FT-Raman system with a motorized stage is ideal to *profile* structural heterogeneity of quenched *melts*, dispersive Raman scattering using red light, which excites electronic states in the conduction band tails, provides reliable VDOS of the *homogenized glasses* to probe elastic phase transitions as shown in Part II. We also measured the optical absorption coefficient of 647 nm radiation in $GeSe_2$ glass and found a value of 9.8/cm, confirming that the radiation essentially serves as a bulk probe of the present Ge-Se glasses.

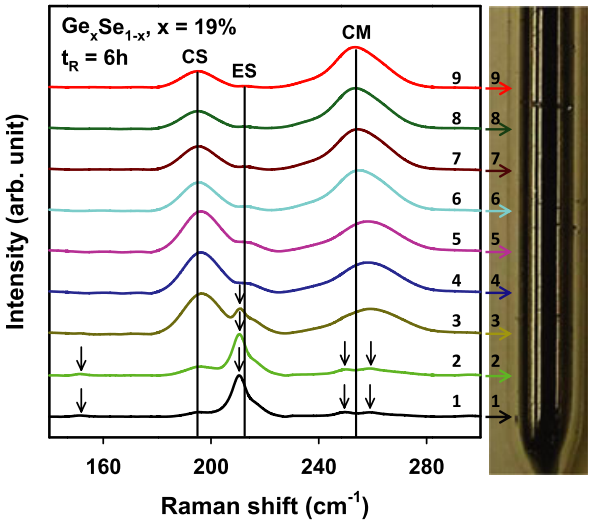

Fig. 2. FT-Raman scattering of a quenched $Ge_{19}Se_{81}$ melt taken at 9 locations along the length of a quartz tube (right panel) after starting materials were reacted at 950°C for 6 h. Glass compositions at locations, 1–3 show narrow modes (see arrows) of α-$GeSe_2$,[16] while those at higher locations (4→8) become steadily Se-richer.

$Ge_{19}Se_{81}$

In the initial stages (t_R = 6 h, Fig. 2) melts were found to be quite heterogeneous. We observe modes[16] of α-$GeSe_2$ at the tube bottom (location 1). The scattering strength of the modes of α-$GeSe_2$ systematically decreases as one moves up the tube from location 1 to 3, and then vanishes at locations 4 and higher. The scattering strength of the Se-chain mode (near 250/cm) increases from location 4 to 9, while that of the symmetric stretch of $GeSe_4$ tetrahedra (200/cm) decreases in the same position range, showing that melts become steadily Ge deficient in going from locations 1 to 9. These spectra when coalesced (Fig. 3a) provide a pictorial view of melt heterogeneity. Continued reaction (t_R = 24 h) of melts (Fig. 3a), lead α-$GeSe_2$ (Fig. 3b) to completely dissolve into melt but only after t_R = 96 h (Fig. 3c) of reaction. At that point melt stoichiometry variation narrows to vary from 17% at location 1 to 21% at location 9. These estimates are based on the scattering strength ratio of the Se-chain mode to the CS mode that is found to vary systematically with x (see Part II). Note that the sequence of colors, which codes sample location in the inset of Fig. 3c closely tracks the Se-chain mode scattering strength,

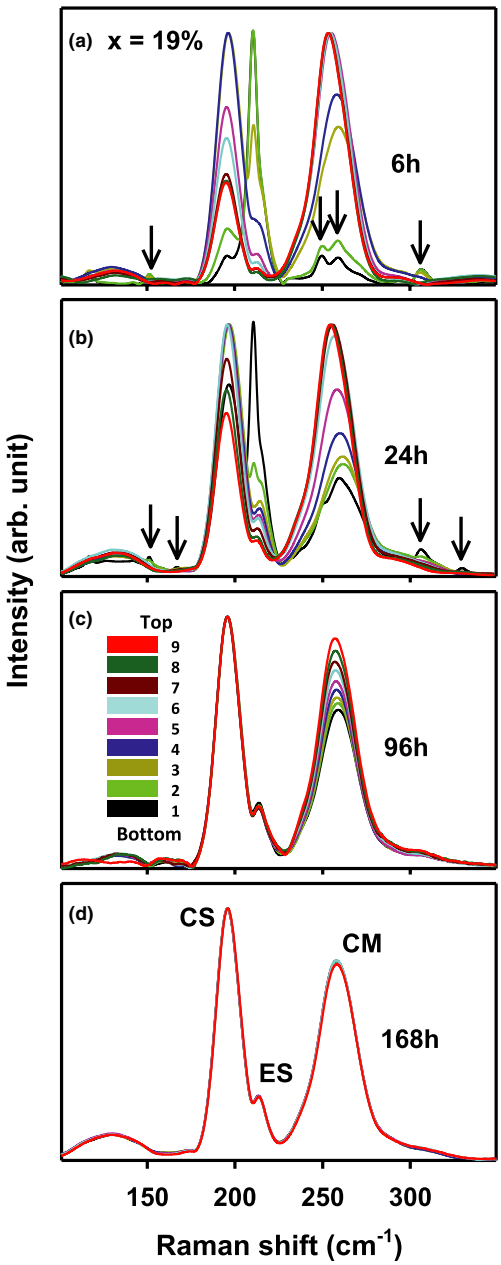

Fig. 3. FT-Raman profiled data of Fig 2 are coalesced in panel (a). Increased reaction times of the starting materials leads (b) after t_R = 24 h, (c) after t_R = 96 h, and (d) after t_R = 168 h, the batch composition to globally homogenize as spectra at the nine locations become identical in (d).

showing that the Se content of glasses steadily increases from location 1 to 9. The FT-Raman software normalizes spectra to the highest peak (Fig. 3c), and for that reason no variations in scattering strength of the CS mode (200/cm) are noted. But a fully homogenized melt is realized only after t_R = 168 h (Fig. 3d) when all the nine Raman spectra coalesce into a single profile. Noteworthy is the fact that scatter in the low frequency range (100–180/cm) (Fig. 3c), near the Se-chain mode, and near the 300/cm (ES) mode also vanishes (Fig. 3d) as melts homogenize. These data show that the small spread in Ge-stoichiometry of 4% prevailing across the melt at t_R = 96 h (Fig. 3c) took an additional 72 h of reaction (Fig. 3d) to completely disappear, and for the melt to homogenize.

$Ge_{15}Se_{85}$

The homogenization behavior of such melts was similar to the one discussed above for $Ge_{19}Se_{81}$ but with a notable change. At a lower Ge content, less of the α-$GeSe_2$ phase is formed at the tube bottom, and after 24 h of reaction nearly most of it dissolved in the melt (Fig. 4b). Continued reaction leads (t_R = 96 h) to melts of increased homogeneity (Fig. 4c) with the variation in Ge-stoichiometry across the melt column narrowing to about 2% (14% at location 1 and 16% at location 9), as suggested by the scattering strength variation of the 200/cm relative to the 250/cm mode. But a fully homogenized melt was realized only after t_R = 168 h (Fig. 4d) when all the 9 Raman spectra coalesced into a single one, and with the scattering strength variation in the low frequency (100–180/cm) and high frequency (320/cm) region also vanishing. These data along with the one at x = 19%, illustrate that the process of homogenization has broadly two steps, one going from Figs. 4a–c leading to the appropriate local structures being formed, and the second step from Figs. 4c–d, resulting in a global homogenization of the melt.

$Ge_{33.33}Se_{66.66}$

At high Ge concentrations new features appear in melts not seen earlier, as illustrated in Figs. 5–7, which reproduce the profiling scans obtained after t_R = 6, 24 and 96 h. Now we observe modes near 170 and 230/cm not seen earlier at lower x. These modes result from Ge-rich amorphous phases, including an ethane-like Ge_2Se_6 unit[41] and a distorted rock-salt GeSe phase[33] that are formed near the bottom of quartz tubes. A few sharp modes are observed at

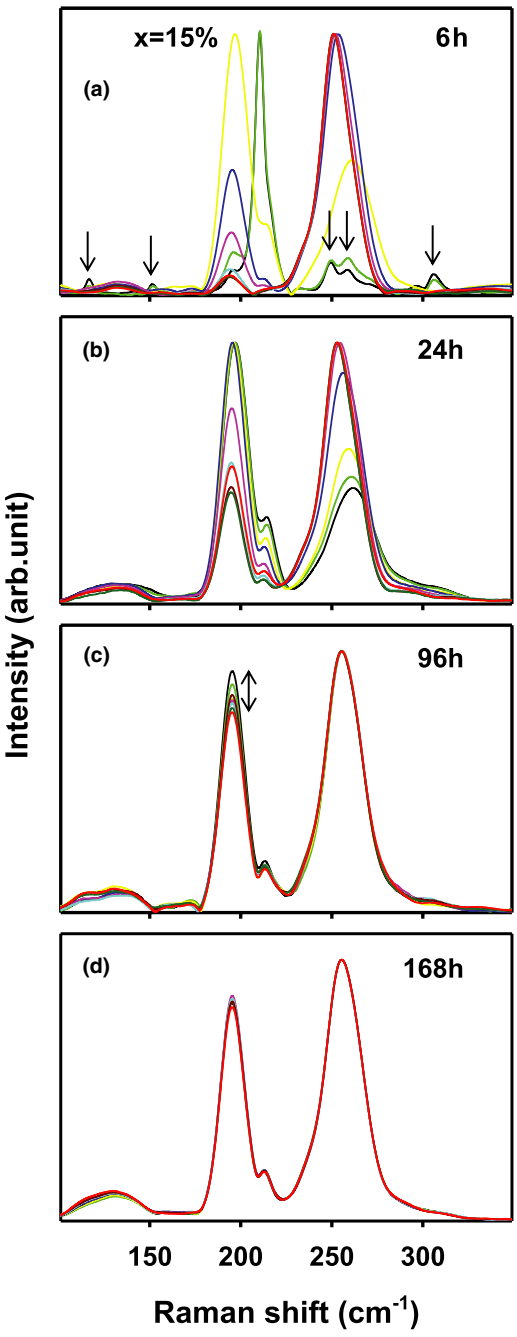

Fig. 4. The homogenization behavior of a melt at x = 19% in Fig 3 was replicated at x = 15% in Fig. 4 with a change that the content of α-$GeSe_2$ phase formed at the bottom was smaller. (c) After 96 h of reaction, the Ge content of the quenched melt steadily is found to increase from location 9–1 as revealed by the color sequence of the CS mode near 200/cm. (d) After t_R = 196 h the melt stoichiometry across the batch homogenized.

location 5 (Fig. 5) toward the center of the melt column, and these are readily identified with those of α-$GeSe_2$. After 24 h of reaction (Fig. 6), modes of the Ge-rich amorphous phases decrease in scattering strength, while those of α-$GeSe_2$ now appear to grow particularly in the lower half of the tube (6, Fig. 6). The upper half of the melt column shows modes of CS and ES units, but with the Ge content of melts steadily decreasing from locations 5 to 9. Continued reaction (t_R = 96 h) of melts, promotes homogeneity (Fig. 8) as the α-$GeSe_2$ phase, and the two Ge-rich amorphous phases reconstruct with the top Se-rich glassy phase but with a surprising observation – a pronounced increase in scattering of low frequency modes (<150/cm). The scattering strength increases as we move toward the melt column center (Fig. 7). The increased low frequency scattering at locations 1–6 in Fig. 7 is not due to a specific mode but rather a general increase in the low frequency(ν) scattering, which is being cut off by the spectral response of the FT-system at ν < 100/cm due to the notch filter. The buildup of low-frequency scattering after 96 h of reaction is the signature of long range network structure

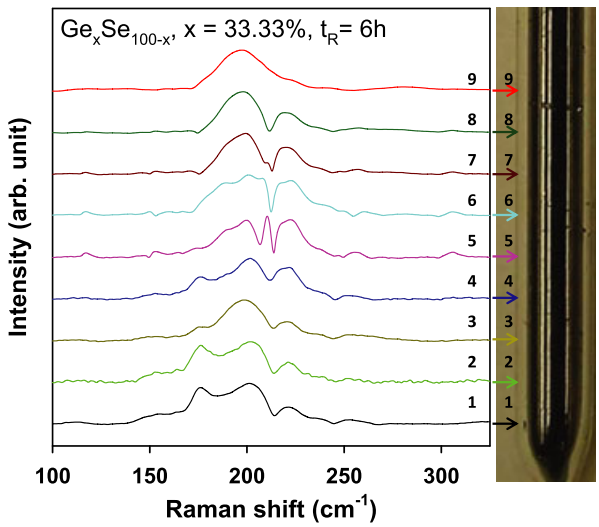

Fig. 5. Raman profiling of $GeSe_2$ melt reacted at 950°C for t_R = 6 h, shows evidence of new features at locations 1→4 not seen earlier; the appearance of new modes near 180/cm (a-Ge_2Se_6) and near 220/cm (a-GeSe) and at location 5 a narrow mode near 210/cm (α-$GeSe_2$[16]). These observations show formation of new Ge-rich amorphous and crystalline phases at the lower end of the tube.

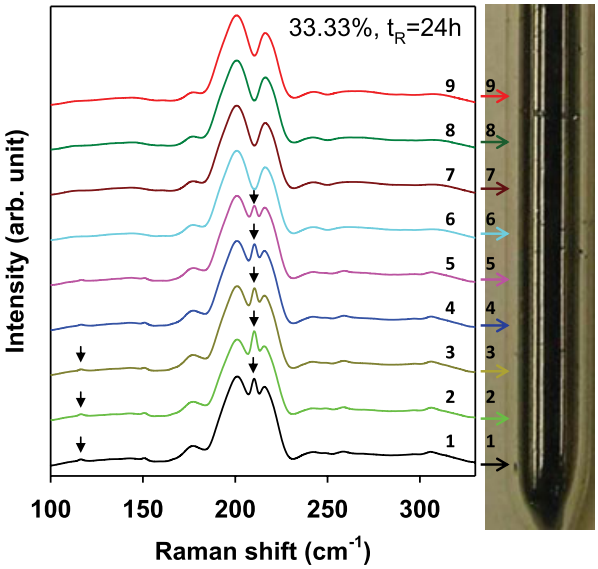

Fig. 6. Continued reaction of the $GeSe_2$ melt at 950°C for t_R = 24 h shows the Ge-rich amorphous Ge_2Se_6 and GeSe phases transform to glassy and c-$GeSe_2$ at locations 1→6, and predominantly g-$GeSe_2$ at locations 7→9.

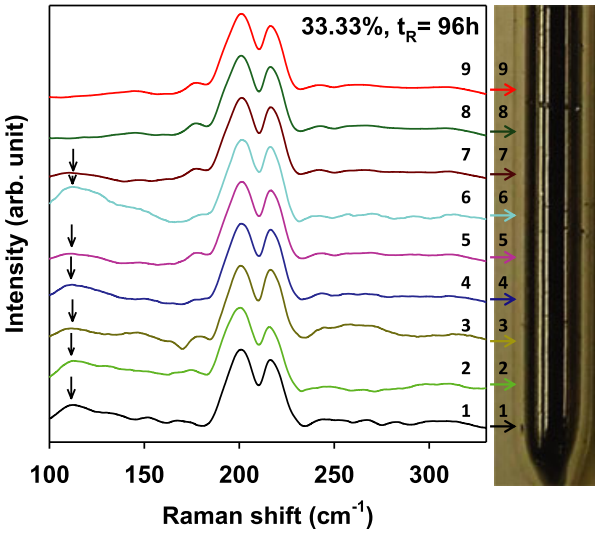

Fig. 7. New features appear in the Raman spectra after the $GeSe_2$ melt is reacted for t_R = 96 h at 950°C- significant low frequency (< 150/cm) scattering appears as α-$GeSe_2$ dissolves in the glassy matrix which becomes the majority phase. In spite of that fact, the resulting melt is far from homogeneous as revealed by the low-frequency scattering (arrow locations).

evolution as Ge-rich nanophases disappear. The data of Fig. 8d, unambiguously show that $GeSe_2$ melt homogenizes globally only after a reaction time t_R of nearly 192 h. These data at x = 33.33% (Fig. 8) along with those at x = 19% (Fig. 3) and at 15% (Fig. 4), reinforce the view that in the 1st step of reaction of the starting materials, characteristic Ge-rich crystalline and amorphous phases form toward the tube bottom. Prolonged reaction at 950°C eventually leads batch composition to globally homogenize in the second step as we comment later.

An interesting observation was made during homogenization of $GeSe_2$ melts. After reacting melts for t_R = 180 h, Raman profiling data showed that the batch had homogenized (Fig. 9) everywhere except for just one location, 7, where α-$GeSe_2$ had formed. Inspection of the sample showed that location 7 coincided with the meniscus cavity tip, a singularity that apparently nucleated crystallization. By rocking the melt for an additional few hours we could completely homogenize the sample.

Laser Spot Size and the Spatial Scale of Melt Homogeneity

The Thermo Nicolet FT-Raman system has in its micro-setting provisions for two laser spot sizes, 250 and 50 μm. In an earlier study[42,43] we had homogenized Ge_xSe_{100-x} melts using a laser spot size of 250 μm, and found homogenization to occur after reacting the starting materials for t_R = 96 h (Fig. 10), i.e., a shorter time than in the present work. However, measurements of the reversibility window in the earlier study[30,42] revealed walls of that window were slopping and wide in relation to the ones observed in the present work (see Part II). Clearly, laser spot size in these Raman profiling experiments intrinsically sets the spatial scale at which melts are probed in these homogenization studies. And it appears dry chalcogenide melts homogenize slowly, and must be homogenized on at least a 50 μm scale to observe their intrinsic physical behavior in compositional studies.

Once homogenized, melts were then separately examined using 647 nm radiation in a dispersive Raman system bringing laser light to a 10 μm laser spot size using a confocal microscope attachment with a 10× objective. In Fig. 11, we compare the Dispersive Raman profiled data on a $GeSe_2$ glass sample taken at 10 μm resolution with FT-Raman profiled data taken

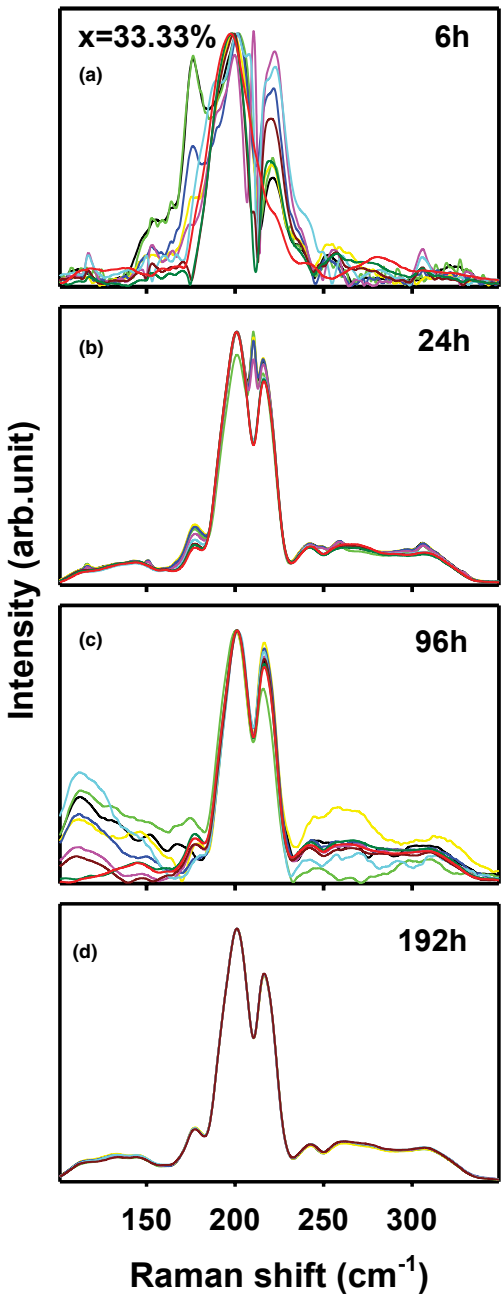

Fig. 8. Summary of Raman profiled data of a $GeSe_2$ melt reacted for t_R of (a) 6 h, (b) 24 h, (c) 96 h, and (d) 192 h. These data show the rather dramatic changes in melt molecular structure as it eventually globally homogenize after t_R = 192 h.

at 50 μm resolution. These data unequivocally show that reaction of melts at 950°C at 168 h leaves them homogenized on a scale of 10 μm.

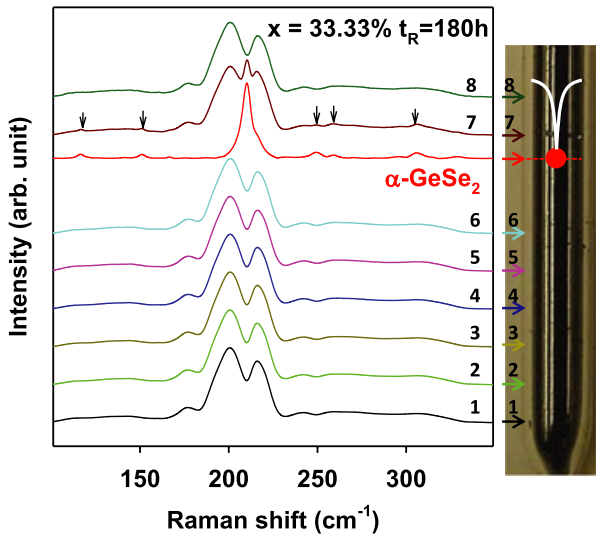

Fig. 9. FT-Raman profiled $GeSe_2$ melt after t_R = 180 h reveals another striking feature- the nucleation of α-$GeSe_2$ at location 7 where the tip of the meniscus had formed on the liquid surface. The singularity is sufficient to nucleate the crystalline phase. Several sharp modes observed in the spectra (see arrows) at position 7 coincide with those of α-$GeSe_2$. We have inserted Raman spectrum of α-$GeSe_2$ between positions 6 and 7.

Melt Size and Reaction Time to Homogenize

Do melt sizes play a role in the kinetics of homogenization? To address the issue we synthesized a ¼-g-sized melt of $Ge_{19}Se_{81}$ and monitored its structural evolution as a function of t_R in FT-Raman profiling experiments. We found the melt homogenized in only 6 h (Fig. 12c) while the 2-g melt took 168 h (Fig. 12b) to homogenize. For comparison, in Fig. 12, we compare Raman profiling results on a 2-g melt with the ¼-g melt both reacted for 6 h. It is abundantly clear from these data that melt sizes play a crucial role in the kinetics of homogenization, and we discuss the issue below.

Rocking of Melts and Homogenization

Once Ge-Se mixtures are first heated to 950°C to initiate reaction of the elements, we noticed a vigorous flow of liquid up and down a quartz tube held vertically. The liquid in question is Se since it melts at 220°C while the chosen reaction temperature is 950°C, substantially higher than the Se melting temperature. For this reason and others, we chose to perform only

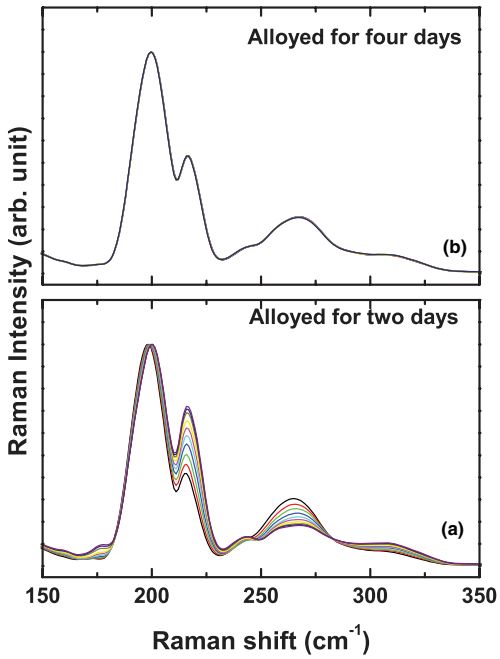

Fig. 10. FT-Raman profiled data on a quenched $Ge_{30}Se_{70}$ melt after reacting the starting materials at 950°C for (a) 2 days and (b) 4 days using a 250 μm laser spot size. Note that after 4 days of reaction, melts were found homogenous when monitored using a 250 μm laser spot size, but not with a 50 μm laser spot size (see Fig. 8), a finding entirely consistent with the reversibility window having sloping walls in the former but rather abrupt ones in the latter glasses. See Part II.

select measurements (at $x = 19\%$ and 25%) of rocking the quartz tube to promote melt mixing. Quartz tubes were positioned horizontally in a muffle furnace, and the furnace rotated continuously in a vertical plane by 45 degrees at a rate of 1/10 cycles per second. After reaction of the elements at 950°C for 48 h, Raman profiling data on these rocked melts showed that the appropriate local structures had formed, i.e., no crystalline phases were observed, suggesting that the first step of homogenization had been speeded up (Figs. 13a and d). However, a significant variation in Ge/Se stoichiometry across the batch composition persisted. Melts were transferred to a box furnace and reacted further in a vertical position. At $t_R = 120$ h, melts were profiled and found still not to be completely homogeneous (Figs. 13b and e). However, at $t_R = 168$ h, melts homogenized as shown in Figs. 13c and f. Note that the lineshape spread near the Se-chain mode (250/cm), in the region of the low frequency band (100–180/cm) and near the ES mode (320/cm) disappeared after 168 h. It appears that it is the slow nanoscale mixing of chalcogenides melts that equalizes the Ge/Se melt stoichiometry across batch compositions globally.

Water as a Dopant in Glasses

We synthesized a pair of samples ($x = 19\%$ and 33.33%) of 2 g each in size, this time using finely powdered (~10 μm) elemental Ge and Se stored in the laboratory ambient environment (45% Relative Humid-

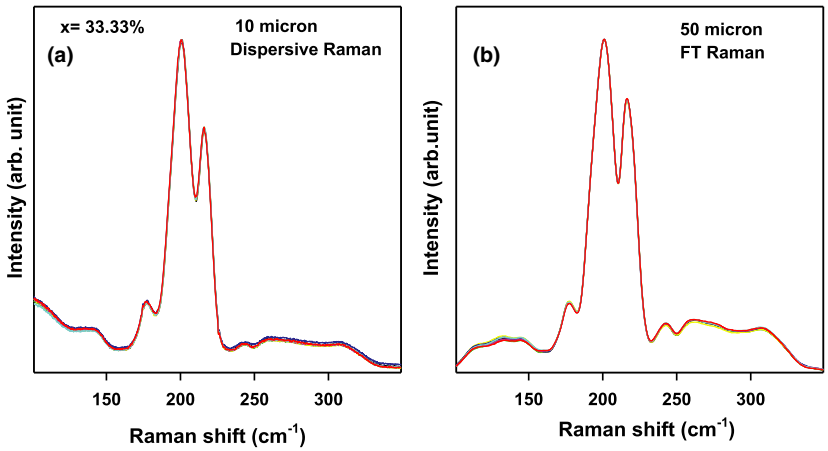

Fig. 11. Raman profiling of a quenched $GeSe_2$ melt monitored (a) using a 10 μm laser spot size in a Dispersive measurement, and (b) using a 50 μm laser spot size in an FT-Raman measurement. These data show that melt homogenized on a 50 μm laser spot size as in (b), are reasonably homogeneous on a finer scale of 10 μm scale as in (a).

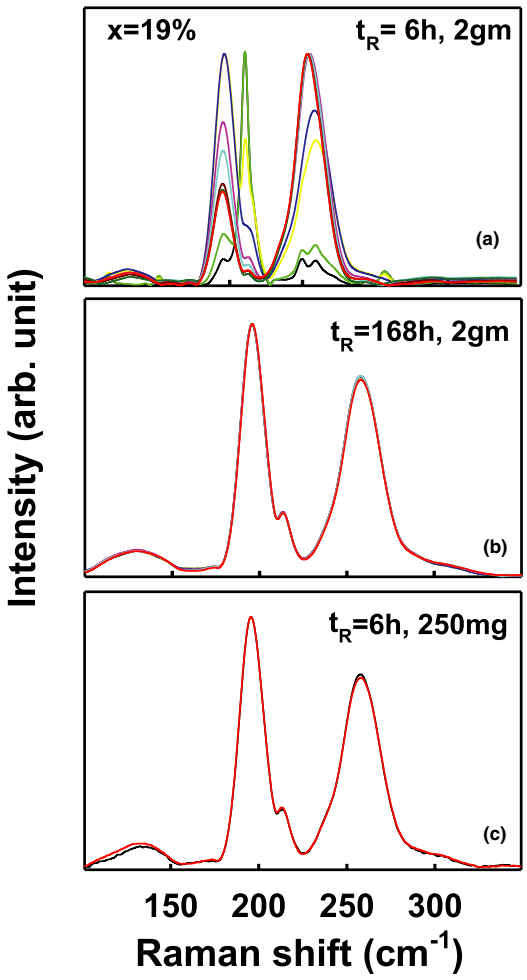

Fig. 12. FT-Raman profiling of a quenched $Ge_{19}Se_{81}$ melt of 2 g in size reacted at 950°C for (a) 6 h and (b) 168 h. Parallel measurements on a much smaller sized (1/4 g) melt reacted at 950°C for 6 h appear in (c). Smaller sized melts homogenize much quicker than larger ones.

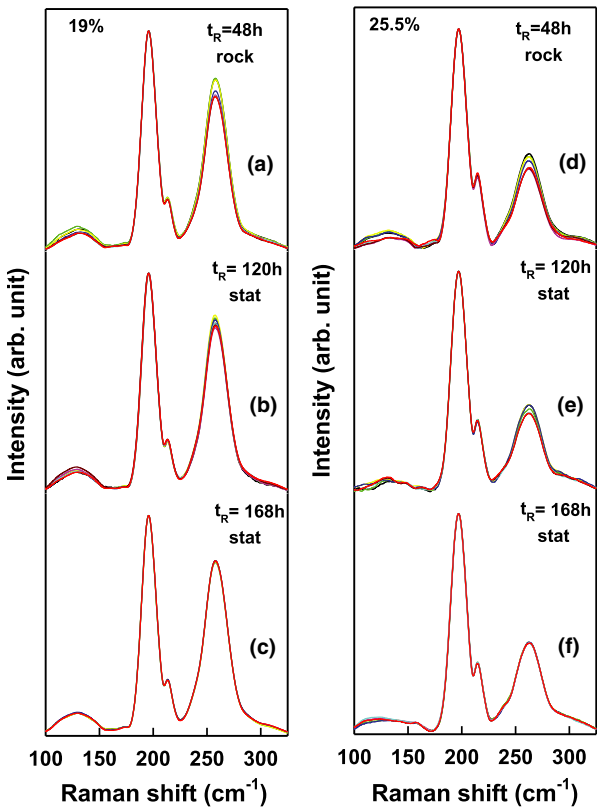

Fig. 13. FT-Raman profiling of a quenched $Ge_{19}Se_{81}$ melt shown in the left panel after (a) being rocked for 48 h, and thereafter held stationary (b) for 120 h (c) 168 h. Parallel results on a quenched $Ge_{25.5}Se_{74.5}$ melt shown in the right panel after (d) being rocked for 48 h, and thereafter held stationary (e) for 120 h and (f) for 168 h. Rocking of melts assists their mixing in the first step of reaction.

ity) for 24 h. We found that a 2-g batch size of finely ground $Ge_{20}Se_{80}$ glass mixture picked up about 4.5 mg in weight after 24 h exposure to laboratory environment. These data suggest an uptake of one water molecule for 85 atoms of the glass. These starting materials were encapsulated in evacuated (10^{-6} Torr) quartz tubes and reacted at 950°C the usual way. Melts were homogenized and Raman profiled. Surprisingly, after reacting such a melt at $x = 19\%$ for only $t_R = 42$ h, we found it homogenized as illustrated in Fig. 14a. The behavior is in sharp contrast to that of dry melts, which took 168 h to completely homogenize (Fig. 3c). A wet melt at $x = 33.3\%$, took 72 h to completely homogenize (Fig. 14c), while a dry one took 192h (Fig. 8d) to do so. These data strongly suggest that water traces speed up the kinetics of melt homogenization rather remarkably.

Dispersive Raman scattering on these wet melts when compared to their dry counterparts show the presence of *residual scattering* as shown in Fig. 15. For example, at $x = 19\%$ (Fig. 15a) we observe that modes of the CS and ES tetrahedra and CM sit on a baseline that is measurably higher than the corresponding modes in the lineshape of dry samples. A parallel behavior was noticed at $x = 33.33\%$ (Fig. 15b). Furthermore, in Fig. 15a, we note that the Se-chain mode scattering strength in a wet sample at $x = 19\%$ is lower than in a dry one (Figs. 3d and 15a). Presence of water

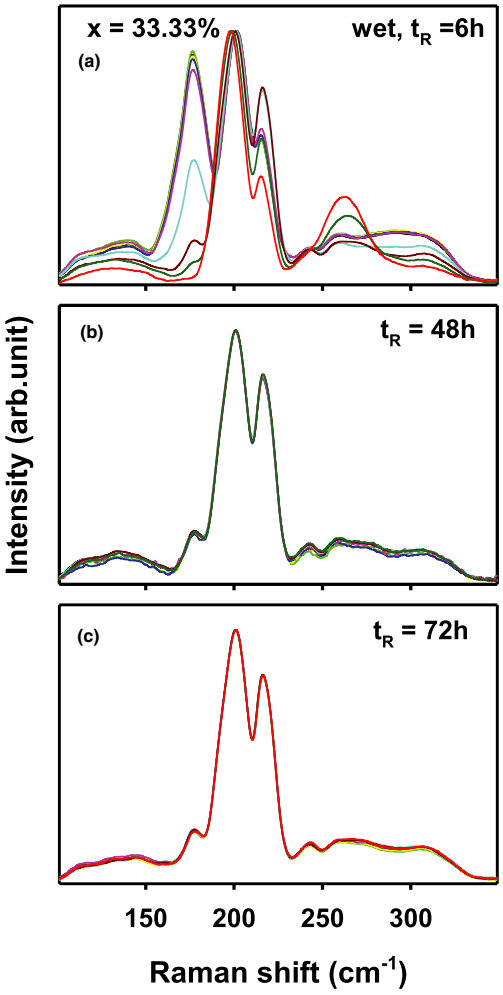

Fig. 14. FT-Raman profiling of a wet quenched $GeSe_2$ melt after starting materials are reacted at 950°C for (a) 6 h (b) 48 h and (c) 72 h. Results on corresponding dry melts appear in Fig 3. Water traces in melts assist Ge crosslinking of the long Se_n chains by depolymerizing them with dangling ends (H, OH).

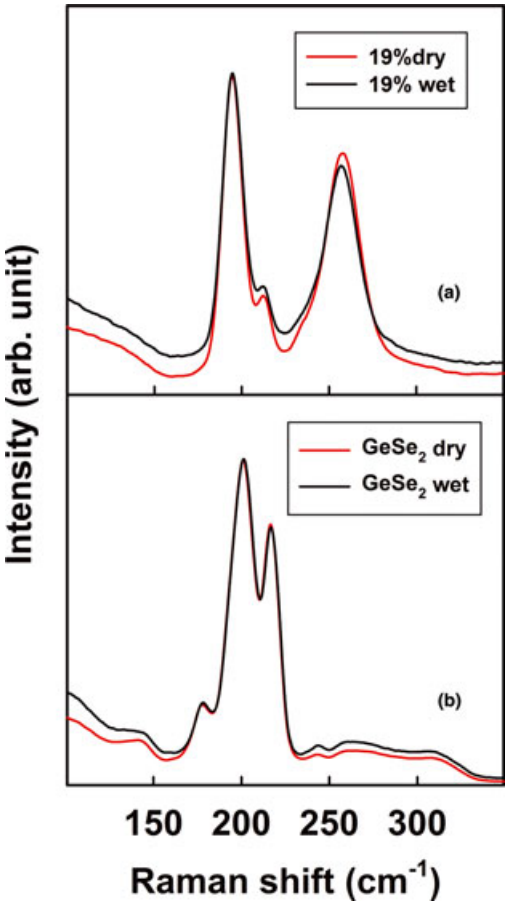

Fig. 15. Dispersive Raman scattering on wet and dry quenched melts of composition (a) $Ge_{19}Se_{81}$ and (b) $GeSe_2$. Wet samples show residual scattering, i.e., baseline counts under the vibrational modes, coming from sample heterogeneity. Also note that in (a) for the Se-rich glass, the scattering strength of the Se_n-chain mode decreases in the wet sample is lower than in the dry one, probably reflecting partial loss of chains due to their de-polymerization by dangling ends.

impurities in melts leads to residual Raman scattering and may alter mode scattering strengths.

Discussion

Melt Homogenization and Nanoscale Mixing

The Raman profiling data presented earlier (Figs. 2–11) provides new insights into physical processes that lead to homogenization of chalcogenides melts. The reaction of elemental Ge with Se in evacuated quartz tubing at 950°C is broadly consistent with *two* steps that underlie the homogenization process of melts.

First Step: Formation of Characteristic Melt Local Structures

In the initial stages, when Ge-Se mixtures are heated to 950°C, the sloshing liquid running up and down the reaction tube is molten Se, (T_m = 221°C), and with increasing reaction time it alloys with Ge.

Because the density of liquid Ge (ρ_{Ge} = 5.60 g/cm^3) exceeds that of Se (ρ_{Se} = 3.99 g/cm^3), in the initial stages the melt at the tube bottom is largely Ge-rich, which may consist of crystalline as well as amorphous phases. In synthesis of $Ge_{15}Se_{85}$ melts, we observed α-$GeSe_2$ to form at the tube bottom (Fig. 4) in the initial stages (t_R = 24–48 h), an illustration of Microscopic heterogeneity (MH). As the Ge content of melts increases (as in $Ge_{19}Se_{81}$), we observe more of the α-$GeSe_2$ to form (Fig. 3) at the tube bottom in the initial stages. In melts at x = 33.33% (Fig. 5), new Ge-rich phases appear in the initial stages besides α-$GeSe_2$. Thus, for example, in the spectra in Fig. 5 we observe modes near 175/cm and near 220/cm, which are replicas of the A_g (170/cm) and B_{2g} (230/cm) phonons of the distorted rocksalt structure of c-GeSe.[33] The feature near 175/cm is a composite of two vibrational modes- one from the distorted rocksalt structure (170/cm) and the other from ethane-like Ge_2Se_6 local structures (180/cm).[41] These Ge-rich phases can be expected to form near the tube bottom (loc 1, 2, and 3) since liquid Ge is heavier than liquid Se, and at 950°C, the reaction temperature used in the present work, occurs predominantly as a tetrahedrally coordinated covalent liquid with little or no vapor pressure resting at the tube bottom. Moving up along the tube, we then observe a mode near 180/cm of ethane-like units (Ge_2Se_6) at locations 5, 6, 7 and a sharp mode near 210/cm from α-$GeSe_2$. Toward the top of the tube, we observe a broad mode near 200/cm, which is the symmetric breathing mode of CS mode of $Ge(Se_{1/2})_4$ tetrahedra. Clearly, the equilibrium phase diagram provides guidance in understanding the phases formed in the initial stages of reaction of Ge with Se in these melts (Fig. 1). These phases contribute to MH as shown by the Raman profiling data (Figs. 3, 4 and 8) presented herein.

Continued heat treatment of melts results in the Ge-rich crystalline and/or amorphous phases to reconstruct with Se-rich regions as appropriate local structures of melts/glasses evolve. These local structures include CS-, ES- tetrahedra, and Se_n-chain fragments.[1,44] At the end of step 1, melts continue to be heterogeneous however, as illustrated in Figs. 3c,4c, and 8c. Melt stoichiometry, measured in terms of Ge content x, typically varies anywhere from 3% to 6% across the length of the liquid column. In Raman scattering (Figs. 3c, 4c and 8c) evidence for such heterogeneity was deduced from the scattering strength ratio of the Se_n-chain mode to the CS mode. In Fig. 3c, for example, we find that melt stoichiometry varies from x = 21% at location 1 (tube bottom) to x = 17% at location 9 (tube top). The 4% spread in Ge content across the length of the tube for a melt of $Ge_{19}Se_{81}$ average stoichiometry is a typical result. Parallel results are observed for $Ge_{15}Se_{85}$ and $GeSe_2$ melts in Figs. 4c and 8c.

Second Step: Nanoscale Mixing and Global Homogenization of a Melt Composition

We view the second step of homogenization to be *nanoscale mixing* as Ge atoms diffuse up and Se atoms down the reaction tube and melts globally homogenize. The process involves a sequence of bond-breaking and bond-forming steps as both Ge and Se diffuse, and concentration gradients dissipate. The case of $GeSe_2$ melts is particularly illustrative (Fig. 7, location 4, 5, and 6) in this respect. We observe growth in scattering near 120/cm, which is evidence of intermediate range network structure evolution. Melts in the lower half of the tube, and especially at locations 3, 4, and 6 appear to display significant low frequency scattering, which we view as evidence of melt structure acquiring a polymeric structure. Here we must remember that a prerequisite for a homogeneous network structure to evolve in the melt is that Ge- and Se-rich regions reconstruct with each other by Ge and Se atoms diffusing respectively to Se-rich and Ge-rich regions. Remarkably, as melts are reacted longer (t_R = 192 h), this appears to be suggested by the spread in Raman scattering strength in the low-frequency and the high frequency range vanishing (compare Fig. 8c and d), and all nine spectra become identical. The result is not peculiar to $GeSe_2$ melts, it is observed in $Ge_{15}Se_{85}$ melts (compare Figs. 3c and d) and also in $Ge_{19}Se_{81}$ (compare Figs. 4c and d). Our experiments show that in dry melts, nanoscale mixing of Ge with Se typically takes about 96 h of reaction time (192–96 h), as the Ge/Se fraction across the 2-g batch composition globally homogenizes. From these data we can estimate a Ge and Se atom diffusion constant (D_{exp}) in liquid $GeSe_2$ at 950°C by using the Einstein relation,

$$D = x^2/6t \qquad (2)$$

Taking a path length (x) of 2.5 cm for Ge and Se atoms to diffuse in an amount of time (t) of 96 h in the reaction tube, one obtains a $D_{exp} = 3 \times 10^{-6}$ cm^2/s.

From MD simulations, the viscosity data on liquid $GeSe_2$,[34] Micoulaut and Massobrio obtained[45,46] a Diffusion constant of Ge and Se of 10^{-5} cm^2/s in liquid $GeSe_2$ at 950°C. The calculated diffusion constant is an order of magnitude lower than the measured one, and at present we are not quite certain why such is the case. In bulk glasses, realized by T_g cycling such homogeneous melts, we have found that the calorimetric properties are quite uniform. In particular, the ΔH_{nr} term appears not to display variations across a batch composition, as noted in glass samples that were synthesized by reacting the starting materials for only 48 h. Our experience reveals that the enthalpy of relaxation ΔH_{nr} deduced from mDSC experiments serves as a rather powerful diagnostic probe of glass sample homogeneity.

Wet Melts Homogenize Quicker than Dry Ones

An important finding of the present work is that *wet* melts synthesized at $x = 19\%$ and 33.33% homogenized much quicker than their dry counterparts. In synthesizing wet melts, the starting elements (Ge, Se) were finely powdered and left in laboratory environment for just 24 h prior to sealing them in evacuated quartz tubes. It is widely known that in such powders the large surface to volume ratio of the small particles leads to adsorption of water from ambient air. And it is difficult to remove water from such starting materials by merely pumping even with a high vacuum line at room temperature.

Viscosity of pure Se melts is found to reduce upon alloying chain terminators such as halogens and *Tl*[47] but it increases measurably upon alloying chain cross-linkers such as Ge, as networks polymerize. Melts containing traces of water vapor will transform bridging Se sites, i.e., Ge-Se-Ge signatures to Ge-[OH]…. [H]-Se-Ge ones, creating [OH] and [H] dangling ends. Monovalent [OH] and [H] species will also serve as Se_n-chain terminators and assist Ge to react with Se_n. For this reason, a wet 19% melt completely homogenizes in only 42 h (Fig. 14a), while its dry counterpart (Fig. 3d) took nearly 168 h to homogenize. A parallel circumstance occurs at $x = 33.33\%$, where a wet melt completely homogenized in 72 h (Fig. 14d) while its dry counterpart took nearly 192 h to completely homogenize (Fig. 8d). These data underscore the crucial role of water impurities in promoting melt nanoscale mixing.

Although it is tempting to add traces of water vapor to accelerate homogenization of melts in the present chalcogenides, the fact is that the presence of water impurities changes the thermal, optical, and mechanical properties of melts/glasses in a deliberate fashion measurably. Thus, we find $T_g(x = 19\%)$ of a dry sample of 171.6°C, is 13.6°C higher than the T_g of its wet counterpart (158°C). A parallel circumstance occurs at $x = 33.33\%$, where T_g of a dry sample (425.7°C) exceeds that of its wet counterpart (T_g = 420.6 °C). The lower T_g*s* of the wet samples compared to dry ones is due to a loss in connectivity of the Ge-Se backbone as dangling ends form. And their presence lowers T_g as network connectivity decreases, a finding that is entirely consistent with SAT.[48] A perusal of the data of Table I also shows that the ΔH_{nr} term at T_g in wet glasses is significantly larger than in dry counterparts. We understand the increased enthalpy of relaxation near T_g as the rocking of dangling [OH] and [H] ends, an entirely non-ergodic process, as glass softens near T_g, and is therefore manifested in the ΔH_{nr} term exclusively. Molar volumes of wet glasses (Table I) are found to be lower than their dry counterparts because of a loss of backbone structure due to cutting of the network. The behavior is observed in oxide glasses as well.[49] Thus, the physical properties of wet glasses are distinctly different from their dry counterparts. These findings lead naturally to the notion that if Ge-Se melts of 2-g size homogenize in less than 68 h of reaction time they could be wet, a speculation that can now be checked by measurement of their physical properties (Table I).

Broader Perspectives

In our discussion so far we have emphasized the role of synthesis on structural homogeneity of melts/glasses. These considerations also have manifestations on dynamics of melts, which are characterized by a stretched exponential relaxation, $A(t) = A_o\exp[-(t/\tau)^{\beta}]$, over many orders of magnitude of time (t). In homogeneous melts/glasses two characteristic stretched exponents, $\beta = 3/5$ and 3/7 are widely observed with the higher value (3/5) resulting when relaxation is mediated by short-range forces (covalent) while the lower one (3/7) when long range forces (Coulomb) come into play.[50] The bimodal βs are characteristic of homogeneous melts/glasses. Recently a cross-over of β from 3/5 to 3/7 was noted[21] in research citation statistics on

Table I. Glass Transition Temperature (T_g), Enthalpy of Relaxation (ΔH_{nr}), Molar Volumes (V_{mol}), and the Reaction Time t_R in Hours Used to Homogenize Melts of Indicated Glass Samples. Our Estimate of Error on Glass Composition x, Based on $T_g(x)$ Variation, is Placed Near 0.1%.

Ge_xSe_{100-x}	T_g (°C) ±2°C	ΔH_{nr} (cal/g) ±0.05 cal/g	V_{mol} (cm^3/mol) ±0.05 cm^3/mol	Reaction time (t_R) (h)
x = 19.0%, dry	171.6	0.36	18.34	168
x = 19.0%, wet	158.0	0.55	18.03	42
x = 33.3%, dry	425.7	0.52	18.87	192
x = 33.3%, wet	420.6	0.74	18.14	72

the Web of Science, in decay of luminescence in crystalline alloy semiconductors, and in relaxation of homogeneous bulk oxide glasses when contrasted to their as-drawn glass sheet counterparts- an issue of much importance in understanding stress-relaxation of these commercial products in industry.[22]

Variations of refractive index with glass composition in chalcogenides (As_2Se_3, As–S, Ge–As–Se) and in soda-lime-silicates have formed the basis of ascertaining homogeneity in industrial applications.[25,51–54] Jensen *et al.*[25] describe the "Homogeneity Index" to quantify glasses, and have emphasized the advantage of image processing methods over refractive index measurements. Industrial processes employing stirrers to homogenize large batches of soda-lime- silicates have been widely used.[55–58] To accurately map refractive index changes across large flat panel displays special optical methods are used.[57] Glass homogeneity issues in industry are pervasive, not restricted to insulating and semiconducting glasses but also extend to glass ceramics and conducting metallic glasses.[59–61]

Conclusions

The functionality of glasses as engineered materials is intimately tied to their chemical composition, structural homogeneity, and state of relaxation or aging, issues that impact both basic science and applications of these materials. Here we have applied an FT-Raman profiling method to track structural heterogeneity of a prototypical chalcogenide melt – Ge_xSe_{100-x}.The process of homogenization is seen to consist of two broad steps. In the first step Ge-rich crystalline and amorphous phases form at the tube bottom and contribute to melt heterogeneity. In the second step, local structures characteristic of melts/glasses emerge and the variation of Ge/Se stoichiometry across a batch composition equalizes as elements diffuse across the melt column, and Raman spectra taken all along the sample length coalesce into *single* profile, with each profile characteristic of a given batch composition x. Homogenization of melts of several other chalcogenides has also been examined in our laboratory, and the results are quite similar to the one discussed herein on the Ge-Se binary. Some of the broad consequences on the basic science of these materials, including the rather *abrupt* onset of rigidity- and stress- phase transitions with glass composition, "x" in homogeneous glasses are addressed in Part II.

Acknowledgments

It is a pleasure to acknowledge conversations with B. Goodman, D. McDaniel, P. Chen, C. Massobrio, J.C. Phillips, J. Mauro, L. Thomas, and S. Mamedov during the course of this work. The present work represents in part the MS Thesis work of S. Bhosle submitted to University of Cincinnati, and was supported in part by NSF grant DMR- 08-53957.

References

1. X. W. Feng, W. J. Bresser, and P. Boolchand, "Direct Evidence for Stiffness Threshold in Chalcogenide Glasses," *Phys. Rev. Lett.*, 78 [23] 4422–4425 (1997).
2. W. Bresser, P. Boolchand, and P. Suranyi, "Rigidity Percolation and Molecular Clustering in Network Glasses," *Phys. Rev. Lett.*, 56 [23] 2493–2496 (1986).
3. D. Sharma, S. Sampath, N. P. Lalla, and A. M. Awasthi, "Mesoscopic Organization and Structural Phases in Network-Forming Ge_xSe_{1-x} Glasses," *Phys. B*, 357 [3–4] 290–298 (2005).

4. S. Mahadevan, A. Giridhar, and A. K. Singh, "Elastic Properties of Ge–Sb –Se Glasses," *J. Non-Cryst. Solids*, 57 [3] 423–430 (1983).
5. P. S. Salmon, and I. Petri, "Structure of Glassy and Liquid $GeSe_2$," *J. Phys.-Condensed Matt.*, 15 [16] S1509–S1528 (2003).
6. P. Boolchand, X. Feng, and W. J. Bresser, "Rigidity Transitions in Binary Ge–Se Glasses and the Intermediate Phase," *J. Non-Cryst. Solids*, 293 348–356 (2001).
7. E. L. Gjersing, S. Sen, and B. G. Aitken, "Structure, Connectivity, and Configurational Entropy of Ge_xSe_{100-x} Glasses: Results From ^{77}Se MAS NMR Spectroscopy," *J. Phys. Chem. C*, 114 [18] 8601–8608 (2010).
8. D. R. Swiler, A. K. Varshneya, and R. M. Callahan, "Microhardness, Surface Toughness and Average Coordination Number in Chalcogenide Glasses," *J. Non-Cryst. Solids*, 125 [3] 250–257 (1990).
9. P. J. Webber, and J. A. Savage, "Some Physical Properties of Ge–As–Se Infrared Optical Glasses," *J. Non-Cryst. Solids*, 20 [2] 271–283 (1976).
10. R. P. Wang, D. Bulla, A. Smith, T. Wang, and B. Luther-Davies, "Structure and Physical Properties of $Ge_xAs_ySe_{1-x-y}$ Glasses With the Same Mean Coordination Number of 2.5," *J. Appl. Phys.*, 109 [2] 023517 (2011).
11. D. L. Pye, A. Montenero, and I. Joseph, *Properties of Glass-Forming Melts*, CRC Press, Boca Raton, FL, 2005, 489pp.
12. S. Bhosle, K. Gunasekera, P. Chen, P. Boolchand, M. Micoulaut, and C. Massabrio, "Meeting Experimental Challenges to Physics of Network Glasses: Assessing the Role of Sample Homogeneity," *Solid State Commun.*, 151 1851–1855 (2011).
13. S. Bhosle, K. Gunasekera, P. Boolchand, and M. Micoulaut, "Melt Homogenization and Self-Organization of Chalcogenide Glasses: Evidence of Sharp Rigidity, Stress and Nanoscale Phase Separation Transitions in the Ge_xSe_{100-x} Binary,"
14. A. Feltz, H. Aust, and A. Blayer, "Glass-Formation and Properties of Chalcogenide Systems XXVI: Permittivity and the Structure of Glasses As_xSe_{1-x} and Ge_xSe_{1-x}," *J. Non-Cryst. Solids*, 55 [2] 179–190 (1983).
15. U. Senapati, and A. K. Varshneya, "Configurational Arrangements in Chalcogenide Glasses: A new Perspective on Phillips' Constraint Theory," *J. Non-Cryst. Solids*, 185 [3] 289–296 (1995).
16. Y. Wang, M. Nakamura, O. Matsuda, and K. Murase, "Raman-Spectroscopy Studies on Rigidity Percolation and Fragility in Ge-(S,Se) Glasses," *J. Non-Cryst. Solids*, 266–269 [Part 2] 872–875 (2000).
17. P. Lucas, E. A. King, O. Gulbiten, J. L. Yarger, E. Soignard, and B. Bureau, "Bimodal Phase Percolation Model for the Structure of Ge–Se Glasses and the Existence of the Intermediate Phase," *Phys. Rev. B*, 80 [21] 214114 (2009).
18. C. Massobrio, M. Celino, P. S. Salmon, R. A. Martin, M. Micoulaut, and A. Pasquarello, "Atomic Structure of the two Intermediate Phase Glasses $SiSe_4$ and $GeSe_4$," *Phys. Rev. B*, 79 [17] 174201 (2009).
19. D. I. Novita, and P. Boolchand, "Synthesis and Structural Characterization of dry $AgPO_3$ Glass by Raman Scattering, Infrared Reflectance, and Modulated Differential Scanning Calorimetry," *Phys. Rev. B*, 76 184205–184212 (2007).
20. M. Takata, M. Tomozawa, and E. B. Watson, "Effect of Water-Content on Transport in $Na_2O.3SiO_2$ Glass," *J. Am. Ceram. Soc.*, 65 [2] 91–93 (1982).
21. G. G. Naumis, and J. C. Phillips, "Bifurcation of Stretched Exponential Relaxation in Microscopically Homogeneousd Glasses," *J. Non-Cryst. Solids*, 358(5) 893–897 (2012).
22. M. Potuzak, R. C. Welch, and J. C. Mauro, "Topological Origin of Stretched Exponential Relaxation in Glass," *J. Chem. Phys.*, 135 214502 (2011).
23. P. K. Gupta, and J. C. Mauro, "Composition Dependence of Glass Transition Temperature and Fragility. I. A Topological Model Incorporating Temperature-Dependent Constraints," *J. Chem. Phys.*, 130 [9] 094503–094508 (2009).
24. J. C. Mauro, and A. K. Varshneya, "Modeling of Rigidity Percolation and Incipient Plasticity in Germanium-Selenium Glasses," *J. Am. Ceram. Soc.*, 90 [1] 192–198 (2007).
25. M. Jensen, L. Zhang, R. Keding, and Y. Yue, "Homogeneity of Inorganic Glasses: Quantification and Ranking," *Int. J. Appl. Glass Sci.*, 2 [2] 137–143 (2011).
26. R. Azoulay, H. Thibierge, and A. Brenac, "Devitrification Characteristics of Ge_xSe_{1-x} Glasses," *J. Non-Cryst. Solids*, 18 [1] 33–53 (1975).
27. C. A. Angell, "Glass Formation and the Nature of the Glass Transitions;" *Insulating and Semiconducting Glasses*, eds., P. Boolchand. World Scientific, Singapore and River Edge, NJ, 1–51, 2000.
28. P. Boolchand, G. Lucovsky, J. C. Phillips, and M. F. Thorpe, "Self-Organization and the Physics of Glassy Networks," *Phil. Mag.*, 85 [32] 3823–3838 (2005).
29. P. Boolchand, D. G. Georgiev, and M. Micoulaut, "Nature of Glass Transition in Chalcogenides," *J. Optoelec. Advanc. Mat.*, 4 [4] 823–836 (2002).
30. P. Boolchand, M. Micoulaut, and P. Chen, "Nature of Glasses;" *Phase Change Materials, Science and Applications*, eds., S. Raoux and M. Wuttig. Springer, Heidelberg, 37–60, 2009.
31. H. Ipser, M. Gambino, and W. Schuster, "The Germanium-Selenium Phase Diagram," *Monatshefte für Chemie/Chemical Monthly*, 113 [4] 389–398 (1982).
32. D. R. Burbank, "The Cryatal Structure of α−Monoclinic Selenium," *Acta Crystallogr. A*, 4 140 (1951).
33. H. R. Chandrasekhar, and U. Zwick, "Raman Scattering and Infrared Reflectivity in GeSe," *Solid State Commun.*, 18 [11–12] 1509–1513 (1976).
34. S. Stolen, T. Grande, and H.-B. Johnsen, "Fragility Transition in $GeSe_2$–Se Liquids," *Phys. Che. Chem. Phy.*, 4 [14] 3396–3399 (2002).
35. M. Jin *et al.* "Origin of Giant Photocontraction in Obliquely Deposited Amorphous Ge_xSe_{1-x} Thin Films and the Intermediate Phase," *Phys. Rev. B (Condensed Matt. Mat. Phys.)*, 78 [21] 214201–214217 (2008).
36. S. G. Bishop, U. Strom, and P. C. Taylor, "Optically Induced Metastable Paramagnetic States in Amorphous Semiconductors," *Phys. Rev. B*, 15 [4] 2278–2294 (1977).
37. M. Abkowitz, and R. C. Enck, "Xerographic Spectroscopy of gap States in Amorphous Semiconductors," *Phys. Rev. B*, 25 [4] 2567–2577 (1982).
38. E. P. O'Reilly, and J. Robertson, "Electronic Structure of Amorphous III–V and II–VI Compound Semiconductors and Their Defects," *Phys. Rev. B*, 34 [12] 8684–8695 (1986).
39. S. Bhosle "Direct evidence for abrupt rigidity and stress transitions in dry and homogeneous bulk GexSe100-x glasses," M.S. Thesis, University of Cincinnati, (unpublished) 2011.
40. T. G. Edwards, and S. Sen, "Structure and Relaxation in Germanium Selenide Glasses and Supercooled Liquids: A Raman Spectroscopic Study," *J. Phys. Chem. B*, 115 [15] 4307–4314 (2011)
41. G. Lucovsky, R. J. Nemanich, and F. L. Galeener, "Amorphous and Liquid Semiconductors;" *Center for Industrial Consultancy and Liason*, eds., W. E. Spear. University of Edinburgh, Edinburgh, 130, 1977.
42. M. T. M. Shatnawi *et al.* "Search for a Structural Response to the Intermediate Phase in Ge_xSe_{1-x} Glasses," *Phys. Rev. B (Condensed Matt. Mat. Phys.)*, 77 [9] 094134 (2008).
43. G. Chen, F. Inam, and D. A. Drabold, "Structural Origin of the Intermediate Phase in Ge–Se Glasses," *Appl. Phys. Lett.*, 97 [13] 131901–131903 (2010).
44. K. Murase, "Vibrational Exciatation in Glasses: Raman Scattering;" *Insulating and Semiconducting Glasses*, eds., P. Boolchand. World Scientific, Singapore and River Edge, NJ, 415–464, 2000.
45. M. Micoulaut and C. Massobrio, "Improving the Structural Description of High-Temperature Liquid $GeSe_2$ From *ab Initio* Molecular Dynamics Simulations," *J. Optoelec. Advanc. Mat.*, 11 [12] 1907–1914 (2009).
46. M. Micoulaut, R. Vuilleumier, and C. Massobrio, "Improved Modeling of Liquid $GeSe_2$: Impact of the Exchange-Correlation Functional," *Phys. Rev. B*, 79 [21] 214205 (2009).
47. J. C. Perron, J. Rabit, and J. F. Rialland, "Impurity Dependence of the Viscosity of Liquid Selenium," *Philosophical Magazine Part B*, 46 [4] 321–330 (1982).
48. M. Micoulaut and G. G. Naumis, "Glass Transition Temperature Variation, Cross-Linking and Structure in Network Glasses: A Stochastic Approach," *Europhys. Lett.*, 47 [5] 568–574 (1999).
49. D. I. Novita, P. Boolchand, M. Malki, and M. Micoulaut, "Elastic Flexibility, Fast-ion Conduction, Boson and Floppy Modes in $AgPO_3$–AgI Glasses," *J. Phys. Condensed Matt.*, 21 205106 (2009).
50. J. C. Phillips, "Microscopic Aspects of Stretched Exponential Relaxation (SER) in Homogeneous Molecular and Network Glasses and Polymers," *J. Non-Cryst. Solids*, 357 [22–23] 3853–3865 (2011).
51. W. A. King, A. G. Clare, and W. C. LaCourse, "Laboratory Preparation of Highly Pure As2Se3 Glass," *J. Non-Cryst. Solids*, 181 [3] 231–237 (1995).

52. M. F. Churbanov, "Recent Advances in Preparation of High-Purity Chalcogenide Glasses in the USSR," *J. Non-Cryst. Solids*, 140 324–330 (1992).
53. N. Prasad, D. Furniss, H. L. Rowe, C. A. Miller, D. H. Gregory, and A. B. Seddon, "First Time Microwave Synthesis of As40Se60 Chalcogenide Glass," *J. Non-Cryst. Solids*, 356 [4142] 2134–2145 (2010).
54. V. V. Golubkov *et al.* "Microinhomogeneities of Glasses of the System PbO–SiO_2," *J. Chem. Phys.*, 110 [10] 4897–4906 (1999).
55. P. K. Bhat, K. L. Bhatia, and S. C. Katyal, "Electrical Conductivity and Photoconductivity of As2S3 PbS Glasses," *J. Non-Cryst. Solids*, 27 [3] 399–409 (1978).
56. M. Cable, and J. Hakim, "A Quantitative Study of the Homogenizing of Glass Melts," *Chem. Eng. Sci.*, 27 [2] 409–415 (1972).
57. Shott, "Homogeneity of Optical Glass," Technical Information: Optics for Devices, 2004. Available at http://www.us.schott.com/advanced_optics/english/download/schott_tie-26_homogeneity_of_optical_glass_july_2004_us.pdf (accessed January 15, 2012).
58. A. R. Cooper, "Kinetics of Mixing in Continuous Glass Melting Tanks," *Glass Technol.*, 7 [1] 2–11 (1966).
59. A. Hernando, M. Vazquez, and J. M. Barandiaran, "Metallic Glasses and Sensing Applications," *J. Phys. E: Sci. Instrum.*, 21 1129–1139 (1988).
60. A. Inoue and N. Nishiyama, "New Bulk Metallic Glasses for Applications as Magnetic-Sensing, Chemical, and Structural Materials," *MRS Bull.*, 32 651–658 (2007).
61. A. Majumdar and S. Jana, "Glass and Glass–Ceramic Coatings, Versatile Materials for Industrial and Engineering Applications," *Bull. Mater. Sci.*, 24 [1] 69–77 (2001).